RSC Advances

COMMUNICATION

View Article Online
View Journal | View Issue

Cite this: *RSC Adv.*, 2014, **4**, 20527

Received 20th February 2014
Accepted 14th April 2014

DOI: 10.1039/c4ra01493f

www.rsc.org/advances

Low-temperature solution-processed Zn-doped SnO_2 photoanodes: enhancements in charge collection efficiency and mobility†

Sambhaji S. Bhande,[a] Dipak V. Shinde,[b] Shoyebmohamad F. Shaikh,[c] Swapnil B. Ambade,[d] Rohan B. Ambade,[d] Rajaram S. Mane,*[ab] Inamuddin,[e] Mu. Naushad[f] and Sung-Hwan Han*[b]

An increase in charge collection efficiency and charge mobility from 78 to 89% and 0.02 to 0.04 $cm^2\ V^{-1}\ s^{-1}$, respectively, in low-temperature solution-processed Zn-doped SnO_2 photoanodes resulted in a two-fold enhancement in power conversion efficiency (PCE) as compared to Zn free SnO_2 photoanodes in dye-sensitized solar cells (DSSCs).

DSSCs have attracted immense interest as promising candidates for the future development of commercially viable solar cells.[1–3] Nanocrystalline TiO_2, ZnO, Nb_2O_5, WO_3 and SnO_2 have widely been envisaged as photoanodes for developing a high performance DSSC to obtain a balance between cost and ease of fabrication, compared with Si-based solar cells.[4] As a DSSC photoanode, TiO_2 has been a dominant material that consistently exhibits PCE as high as ~12%.[5] Analogous to TiO_2, ZnO has also been explored largely due to its similar band gap energy (E_g = 3.2 eV) and electronic energy levels. While the high electron mobility (μ) of ZnO (>200 $cm^2\ V^{-1}\ S^{-1}$) is certainly an advantage, its instability in acidic dyes restricts the electron injection rate from the sensitizer (dye) to ZnO by forming an insulating surface agglomerative layer.[6] Another chemically stable alternative, SnO_2 also possesses relatively high μ (~100–200 $cm^2\ V^{-1}\ s^{-1}$) as compared to TiO_2 (~10^{-2} $cm^2\ V^{-1}\ S^{-1}$).[7] However, one major disadvantage with SnO_2-based DSSC is its tendency to exhibit a relatively low open circuit voltage (V_{oc}). This is due to its 300 mV positively located conduction band level.[8] The inferior photovoltaic properties of SnO_2 are additionally attributed to faster electron recombination kinetics and the poor dye uptake associated with the low isoelectric point.[9] Grätzel *et al.*[10] demonstrated a significant improvement in photovoltaic parameters by covering the mesoporous SnO_2 with a thin shell of ZnO. Nevertheless, this chemically unstable component (ZnO) in the composite is a challenging issue that needs to be resolved. Previously, we reported that employing dual photosensitization can effectively suppress the agglomeration of ZnO nanoparticles.[11] Thus, the most significant challenge is to complement the advantages of the present photoanode materials to construct a compound structure that is chemically stable and possesses higher charge collection kinetics for efficient PCE in DSSCs. In this context, the chemically stable Zn-doped SnO_2 can be a good alternative since the effective ionic radius of Zn^{2+} (74 pm) is close to that of Sn^{4+} (69 pm), and thus, it is expected that Zn^{2+} ions can easily be incorporated into the lattice of SnO_2 to offer fascinating electronic properties collectively. Moreover, the Zn-doped films exhibit an elevated electron Fermi level, which may enhance band bending to lower the density of empty trap states.[12]

In this communication, we present a remarkable 2 fold enhancement in the photovoltaic performance of DSSCs containing chemically synthesized upright-standing Zn-doped SnO_2 nanoplates as photoanodes that exhibit high charge collection efficiency and dramatically reduced charge transport resistance as compared to Zn-free SnO_2 photoanodes with an impressive overall PCE of 4.87%. The obtained PCE is by far the highest for low temperature chemically synthesized SnO_2-based DSSCs.[13] This work is in continuation of our research focusing on the low temperature chemical synthesis of DSSC photoanodes.[14] A low temperature chemical synthesis route is extremely advantageous as it paves opportunities for facile and commercially viable scalable synthesis. Various Zn-doped SnO_2 photoanodes were synthesized using a simple chemical bath

[a]*Centre for Nanomaterials & Energy Devices, School of Physical Sciences, SRTM University, 431606, Nanded, India. E-mail: rsmane_2000@yahoo.com*

[b]*Department of Chemistry, Hanyang University, Seongdong-gu, 133791 Seoul, Korea. E-mail: shhan@hanyang.ac.kr*

[c]*Clean Energy Research Center, Korea Institute of Science and Technology, Seoul 130-650, Korea*

[d]*School of Semiconductor and Chemical Engineering, Chonbuk National University, Duckjin-dong 664-14, Jeonju 561-756, Korea*

[e]*Department of Applied Chemistry, Faculty of Engineering and Technology, Aligarh Muslim University, Aligarh 202002, India*

[f]*Advanced Materials Research Chair, Department of Chemistry, College of Science, Bld#5, King Saud University, Riyadh, Saudi Arabia*

† Electronic supplementary information (ESI) available: Experimental procedures with structural characterizations and supplementary figures (Fig. S1–S6) in addition to tables (T1–T4). See DOI: 10.1039/c4ra01493f

deposition method at 70 °C and termed as A–E with increasing Zn-doping concentration at successive intervals of 1 wt% starting from 0 wt% for A and 4 wt% Zn-doping for photoanode E. The detailed synthesis procedure (with elemental mapping) is presented in ESI† (Table 1). The XRD spectra (Fig. 1) of all photoanodes confirm the tetragonal rutile structure of SnO_2 (file: 41-1445).

For Zn-doped SnO_2 photoanodes, no other crystalline phase and peaks of impurities were detected (Fig. 1, spectra A–E), indicating the formation of neither separate SnO_2/ZnO nor a $Zn_xSn_{1-x}O_2$ composite structure. To investigate the effect of Zn^{2+} ion doping on the crystallinity of SnO_2, (110), (200), and (211) diffraction peaks are monitored. Spectra (B–E) of Fig. 1 reveal that with an increase of Zn wt%, the 2θ values shift by 0.17°, 0.244° and 0.144°, respectively, as compared to those of pristine SnO_2. This clearly proves that Zn^{2+} ion incorporation has led to a lattice deformation in the Zn-doped SnO_2. Moreover, upon Zn-doping, the photoelectron peaks for Sn $3d_{5/2}$ and Sn $3d_{3/2}$ in the X-ray photoelectron spectroscopy (XPS) spectra (Fig. S2b, ESI†) appear to have decreased from 487.96 eV to 486.02 eV and 497 eV to 494.97 eV, respectively. The O 1s transition peak (Fig. S2c, ESI†) is shifted towards the lower binding energy by 2.01 eV from 531.98 eV to 529.97 eV. Also, the strong Zn $2p_{3/2}$ peak (Fig. S2d, ESI†) at the binding energy of 1056 eV further confirms the presence of Zn in the SnO_2 matrix.

The FE-SEM images of pristine and 0–4 wt% Zn-doped SnO_2 photoanodes (Fig. 2) reveal a clear change in the parent surface morphology after Zn-doping. The width of an individual pristine nanosheet was found to be 15–20 nm; it increased to 30–60 nm for Zn-doping of 0–4 wt%. This suggests that Zn-doping leads to a significant change in the morphology of the parent nanostructure (Fig. 2a), with a distinct change in roughness with increasing Zn concentration (Fig. 2b–d). It is expected that the newly formed rough structures must aid in superior dye adsorption. This interconnected network of nanoplates should offer mechanical strength along with rapid electron transport pathways due to the minimized grain boundaries. With a further increase in Zn concentration of more than 3 wt%, the nanoplates tend to bend. This may be due to the lower mechanical strength of the upright standing SnO_2 nanoplates developed due to the breaking of bonds after excessive Zn incorporation.

Fig. 3a shows the *J–V* characteristics of DSSCs (fabricated as per the structure depicted in Fig. 3a) for pristine and Zn-doped

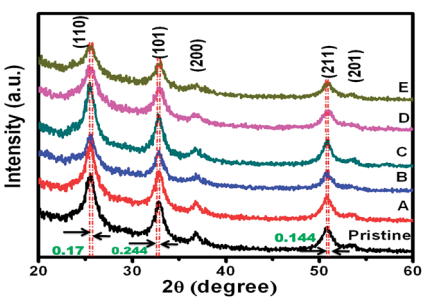

Fig. 1 XRD spectra of pristine and Zn-doped SnO_2 nanoplates.

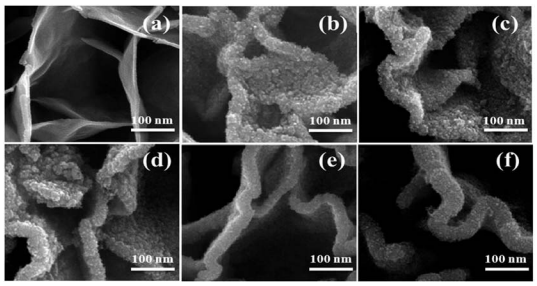

Fig. 2 FE-SEM images of (a) pristine SnO_2, (b) after $TiCl_4$ surface treatment, and (c–f) 1–4 wt% Zn-doped SnO_2 photoanodes.

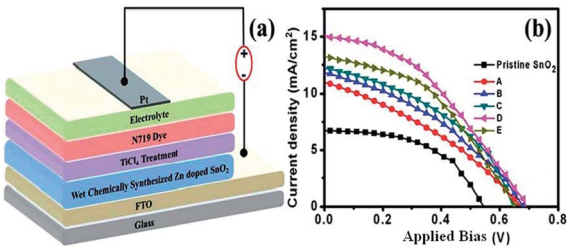

Fig. 3 (a) Device structure and (b) *J–V* curves of all DSSCs under 1 sun illumination.

SnO_2 photoanodes. It is observed that the Zn doping of SnO_2 has a significant impact on DSSC performance. The detailed photovoltaic parameters are summarized in Table 2 (ESI†). DSSCs comprising a pristine SnO_2 photoanode exhibited a short-circuit current density (J_{sc}) of 6.73 mA cm^{-2}, V_{oc} of 0.55 V and a fill factor (*ff*) of 0.51, which itself is an improvement from our previously reported PCE of 0.37% for a pristine SnO_2 photoanode sensitized with dye.[13b] However, PCE increased to 2.54% after $TiCl_4$ treatment because of the pronounced increase in J_{sc} and V_{oc} although ff dropped. This is attributed to the increase in roughness induced by the $TiCl_4$ treatment that eventually increased the uptake of dye and decreased the electron/electrolyte recombination.[15]

In DSSCs of Zn-doped SnO_2 photoanodes, an exponential increase in photovoltaic performance with a Zn doping level of up to 3 wt% is observed. A maximum PCE of 4.87% is achieved for DSSCs having 3 wt% of Zn-doped SnO_2 photoanode, which is about two times higher than that of DSSCs of pristine SnO_2 photoanodes. The increased photovoltaic performance is majorly due to the enhancement in J_{sc}. This is attributed to the enhanced charge-generation efficiency; suppressed electron recombination (explained later using EIS analyses), and higher dye loading, as compared to pristine SnO_2 photoanodes.[16] For comparison, PEC results of SnO_2 photoanodes synthesized using other methods are given in Table 3 of ESI.† The incident photon-to-electron conversion efficiencies (IPCE) of pristine and Zn-doped SnO_2 photoanodes are shown in Fig. S5, ESI.† A considerable change in IPCE measurements after $TiCl_4$ treatment is obtained, which in fact, is significantly less than that in the case of the wet chemically synthesized SnO_2–$TiCl_4$.[13b] However, with the Zn-doping, IPCE values and the wavelength

range are substantially increased. The IPCE value is increased from 30% to 56% (nearly double), which can be attributed to the Zn-doping effect, consistent with *J–V* measurements. A decrease in IPCE at a higher Zn-doping level is due to the negative mass/agglomeration effect of ZnO with SnO_2.[17]

A UV-vis spectroscopy investigation, as shown in Fig. S4 (ESI†), revealed a proportionally higher increase in the optical density at higher wavelengths, strongly indicating increased dye loading after Zn-doping. The dye-loading experiments revealed that the dye loading amounts are increased by 152 and 350%, respectively, for pristine and 3 wt% Zn-doped SnO_2. The suppressed electron recombination is evident from the *J–V* spectra of DSSCs measured under a forward bias potential in the dark, as shown in Fig. S3 (ESI†). The dark current onset of a pristine SnO_2 photoanode occurred at a low forward bias, indicating faster electron-recombination kinetics.[18] In order to analyze the electron transport behavior in the DSSCs, electrochemical impedance spectroscopy (EIS) measurements were performed, which distinguished the charge transport resistance (R_{ct}) from the chemical capacitance of the device.

The equivalent circuit used for EIS measurements and EIS data with electronic parameters are presented in Fig. S6 and Table 4 (ESI†). The Nyquist plots shown in Fig. 4a measured under 1 sun conditions for all DSSCs at the respective V_{oc} conditions clearly reveal lower R_{ct} for the 3 wt% Zn-doped SnO_2 photoanode, resulting due to the reduction of trap states for photogenerated electrons. The EIS measurements revealed higher μ for Zn-doped photoanodes than that of the pristine photoanode, indicating favorable electron transport through a longer distance with less diffusive hindrance after Zn-doping. The variation of diffusion length (L_n) and μ with respect to Zn doping is presented in Fig. 4b. A further increase in the Zn^{2+} ion concentration above 3 wt% in the solution starts deceleration in the L_n value. This is accomplished with a significant increase in the number of bond deformations and the generation of more trap states within the photoanode.[19] The increasing trend of the μ value (Table 4, ESI†) with Zn intercalation in the SnO_2 matrix is clearly noticed (from 0.022 $cm^2 V^{-1} s^{-1}$ to 0.04 $cm^2 V^{-1} s^{-1}$ for pristine and 3 wt% Zn-doped SnO_2 photoanodes, respectively). Zn-doping also resulted in a decrease in the electron transit time (τ_d) (Fig. 4c) from 0.01 to 0.06 s for the pristine and the 3 wt % Zn-doped SnO_2 photoanodes, respectively. The decrease in τ_d proved the minimization of the trapping states, facilitating the effective transport of photogenerated electrons. The mean electron lifetime (τ_n) calculated in all DSSCs using EIS is presented in Table 4, ESI.† Fig. 4d represents the plot of variation of τ_n and PCE of the DSSCs with varying Zn-doping concentrations. The τ_n of the doped photoanode is smaller than that for the undoped photoanode. However, with Zn-doping, the τ_n values are nearly one order of magnitude greater than the corresponding τ_d values, justifying that Zn-doping can minimize the trapping–detrapping processes. The charge collection efficiency (η_{cc}) is found to increase from 78.45% to 89.32% for the undoped and the 3 wt% Zn-doped SnO_2 photoanodes. With a further increase in the Zn-doping, η_{cc} is reduced to 84.76% and τ_d is increased to 0.06 s.

In summary, a low-temperature (70 °C) wet chemical solution method was carried out for the synthesis of Zn-doped SnO_2 photoanodes. DSSCs fabricated with the photoanodes of optimized Zn-doping (3 wt%) exhibited an overall PCE of 4.87% and IPCE of 56%, which is two-fold order higher than the undoped SnO_2 photoanodes. The shortening of the electron transit time after Zn-doping and increased charge collection efficiency proved to be advantageous for the high performance obtained in this work.

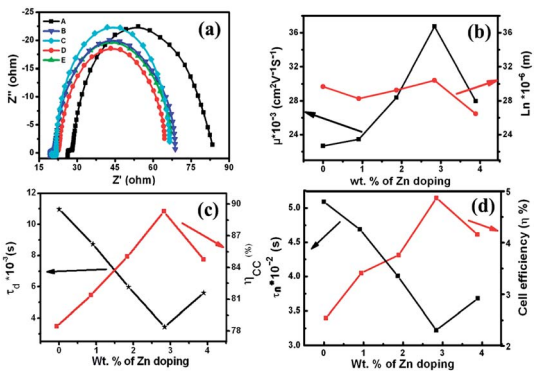

Fig. 4 (a) Nyquist plots, dependence of (b) electron mobility and diffusion length, (c) charge collection efficiency and transit time and (d) electron life time and cell efficiency with Zn-doping.

Acknowledgements

This research was financially supported by: (a) King Saud University, Deanship of Scientific Research, College of Science Research Center and (b) Basic Science Research Program through the National Research Foundation of Korea (NRF) funded by the Ministry of Education (2013009768).

Notes and references

1 B. O'Regan and M. Grätzel, *Nature*, 1991, **353**, 737.
2 P. Wang, S. M. Zakeeruddin, J. E. Moser, M. K. Nazeeruddin, T. Sekiguchi and M. Grätzel, *Nat. Mater.*, 2003, **2**, 402.
3 F. Sauvage, F. Di Fonzo, A. L. Bassi, C. S. Casari, V. Russo, G. Divitini, C. Ducati, C. E. Bottani, P. Comte and M. Grätzel, *Nano Lett.*, 2010, **10**, 2562.
4 Y. C. Qiu, W. Chen and S. H. Yang, *Angew. Chem., Int. Ed.*, 2010, **49**, 3675.
5 A. Yella, H.-W. Lee, H. N. Tsao, C. Yi, A. K. Chandiran, Md. K. Nazeeruddin, E. W.-G. Diau, C.-Y. Yeh, S. M. Zakeeruddin and M. Grätzel, *Science*, 2011, **334**, 629.
6 Q. F. Zhang, C. S. Dandeneau, X. Y. Zhou and G. Z. Cao, *Adv. Mater.*, 2009, **21**, 4087.
7 M. S. Arnold, P. Avouris, Z. W. Pan and Z. L. Wang, *J. Phys. Chem. B*, 2002, **107**, 659.
8 S. S. Bhande, G. A. Taur, A. V. Shaikh, O.-S. Joo, M.-M. Sung, R. S. Mane, A. V. Ghule and S.-H. Han, *Mater. Lett.*, 2012, **79**, 29.
9 A. Kloke, F. von Stetten, R. Zengerle and S. Kerzenmacher, *Adv. Mater.*, 2011, **23**, 4976.
10 A. Kay and M. Grätzel, *Chem. Mater.*, 2002, **14**, 2930.
11 T. Ganesh, R. S. Mane, G. Cai, J.-H. Chang and S.-H. Han, *J. Phys. Chem. C*, 2009, **113**, 7666.

12 K.-P. Wang and H. Teng, *Phys. Chem. Chem. Phys.*, 2009, **11**, 9489.
13 (*a*) D. V. Shinde, I. Lim, C. S. Kim, J. K. Lee, R. S. Mane and S. H. Han, *Chem. Phys. Lett.*, 2012, **542**, 66; (*b*) D. V. Shinde, R. S. Mane, I.-H. Oh, J. K. Lee and S.-H. Han, *Dalton Trans.*, 2012, 10161.
14 S. B. Ambade, R. B. Ambade, R. S. Mane, G.-W. Lee, S. Md. F. Shaikh, S. A. Patil, O.-S. Joo, S.-H. Han and S.-H. Lee, *Chem. Commun.*, 2013, **49**, 2921.
15 B. C. O'Regan, J. R. Durrant, P. M. Sommeling and N. G. Bakker, *J. Phys. Chem. C*, 2007, **111**, 14001.
16 H. J. Snaith and C. Ducati, *Nano Lett.*, 2010, **10**, 1259.
17 (*a*) S. B. Ambade, R. S. Mane, A. V. Ghule, M. G. Takawale, A. Abhyankar and B. Cho, *Scr. Mater.*, 2009, **61**, 12–15; (*b*) R. S. Mane, W. J. Lee, H. M. Pathan and S. H. Han, *J. Phys. Chem. B*, 2005, **109**, 24254.
18 S. Ito, P. Liska, P. Comte, R. Charvet, P. Pechy, U. Bach, L. Schmidt-Mende, S. M. Zakeeruddin, A. Kay, M. K. Nazeeruddin and M. Grätzel, *Chem. Commun.*, 2005, 4351.
19 P. Sun, L. You, Y. Sun, N. Chen, X. Li, H. Sun, J. Ma and G. Lu, *CrystEngComm*, 2012, **14**, 1701–1708.